1-3-2022

# Coastal paleogeography of the Pacific Northwest, USA, for the last 12,000 years accounting for three-dimensional earth structure

Jorie Clark

Jay R. Alder

Marisa Borreggine

Jerry X. Mitrovica

Konstantin Latychev

Quaternary International 638-639 (2022) 197–204

Contents lists available at ScienceDirect

Quaternary International

journal homepage: www.elsevier.com/locate/quaint

# Coastal paleogeography of the Pacific Northwest, USA, for the last 12,000 years accounting for three-dimensional earth structure

Jorie Clark [a,*], Jay R. Alder [b], Marisa Borreggine [c], Jerry X. Mitrovica [c], Konstantin Latychev [c]

[a] College of Earth, Ocean, and Atmospheric Sciences, Oregon State University, Corvallis, OR, 97331, USA
[b] U.S. Geological Survey, Oregon State University, 104 CEOAS Admin Building, Corvallis, OR, 97331, USA
[c] Department of Earth and Planetary Sciences, Harvard University, Cambridge, MA, 02138, USA

ARTICLE INFO

*Keywords:*
Sea level
Submerged archaeology
Coastal paleogeography

ABSTRACT

Predictive modeling of submerged archaeological sites requires accurate sea-level predictions in order to reconstruct coastal paleogeography and associated geographic features that may have influenced the locations of occupation sites such as rivers and embayments. Earlier reconstructions of the paleogeography of parts of the western U.S. coast used an assumption of eustatic sea level, but this neglects the large spatial variations in relative sea level (RSL) associated with glacial isostatic adjustment (GIA) and tectonics. Subsequent work using a one-dimensional (1-D) solid Earth model showed that reconstructions that accounted for GIA result in significant differences from those based on eustatic sea level. However, these analyses neglected the complex three-dimensional (3-D) solid Earth structure associated with the Cascadia subduction zone that has also strongly influenced RSL along the Oregon-Washington (OR-WA) coast, requiring that the paleogeographic reconstructions must also account for this effect. Here we use RSL predictions from a 3-D solid Earth model that have been validated by RSL data to update previous paleogeographic reconstructions of the OR-WA coast for the last 12 kyr based on a 1-D solid Earth model. The large differences in the spatial variations in RSL on the OR-WA continental shelves predicted by the 3-D model relative to eustatic and 1-D models demonstrate that accurate reconstructions of coastal paleogeography for predictive modeling of submerged archaeological sites need to account for 3-D viscoelastic Earth structure in areas of complex tectonics.

## 1. Introduction

Global mean sea level (GMSL) (also referred to as "eustatic" sea level) has varied throughout the Quaternary largely due to the repeated growth and decay of ice sheets, and has been below the present-day level for ~90% of this period (Lambeck et al., 2002; Lisiecki and Raymo, 2005). Local sea-level variations caused changes in coastal paleogeography that influenced coastal migration routes (Goebel et al., 2008; Lambeck et al., 2011) and the locations of sites of human settlement, many of which are now submerged (Bailey et al., 2020b). These submerged coastal settings would have provided productive marine resources that may have supported large populations who then migrated inland, influencing the material and societal culture of existing and subsequent populations there (Bailey and Milner, 2002; Erlandson, 2001).

Because older sea-level fluctuations are likely to have eroded most submerged sites, many studies have focused on sea-level changes since the Last Glacial Maximum (LGM, ~26–19 ka) when the preservation potential of these sites is greatest (Bailey et al., 2020b; Benjamin and Bailey, 2017; Hale et al., 2021; Joy, 2019, 2020; McLaren et al., 2019; Veth et al., 2020). A common approach to reconstruct coastal paleogeography since the LGM has been to uniformly lower sea level by the amount suggested from reconstructions of eustatic change (Fleming et al., 1998) or from far-field sea-level records (Bard et al., 1996; Fairbanks, 1989) which are assumed to represent GMSL (Anderson et al., 2010, 2013; Davis et al., 2004; Kennett et al., 2008). Deglacial sea-level rise at any given location, however, differed from this eustatic assumption because of deformational, gravitational, and rotational effects (henceforth glacial isostatic adjustment, GIA) associated with the redistribution of mass from melting ice sheets to the oceans (Clark et al., 1978; Milne and Mitrovica, 2008). This relative sea-level (RSL; i.e., sea level measured with respect to the surface of the solid Earth) change was particularly variable spatially in areas close to the ice sheets, where GIA effects can be significant relative to GMSL changes. In areas of retreating

* Corresponding author.
*E-mail address:* clarkjc@geo.oregonstate.edu (J. Clark).

https://doi.org/10.1016/j.quaint.2022.01.003
Received 6 September 2021; Received in revised form 21 December 2021; Accepted 3 January 2022
Available online 6 January 2022

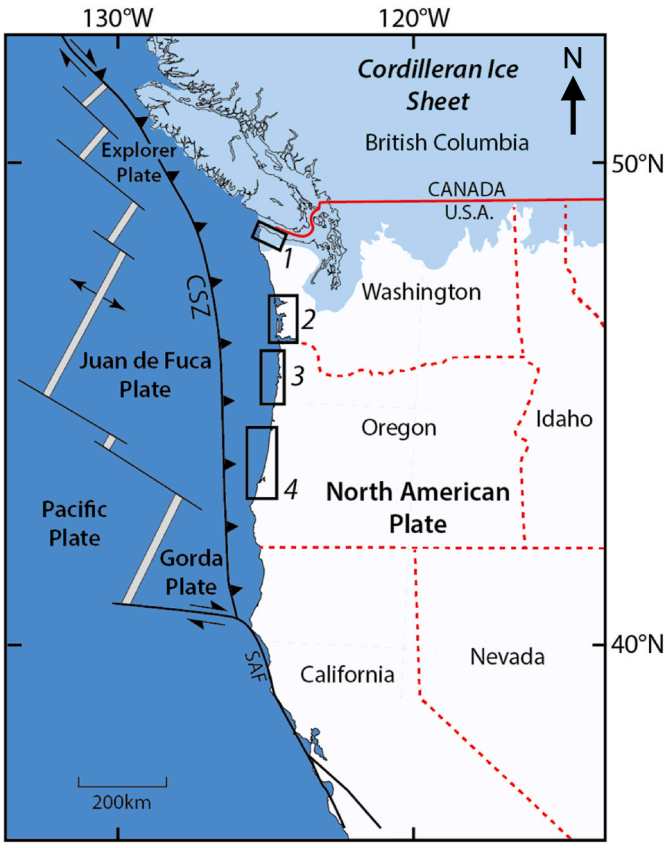


**Fig. 1.** Location map of Cascadia subduction zone (CSZ), San Andreas Fault (SAF), tectonic plates and boundaries, and sites 1, 2, 3, and 4 along the Oregon and Washington coasts referred to in this study.

ice cover, post-glacial rebound of the crust and a weakening of the gravitational effect of the ice sheets can lead to a sea-level fall that dominates the GMSL rise. In contrast, beyond ice-sheet margins, a subsidence of the crust within the so-called "peripheral bulge" of the ice sheets (the uplifted region surrounding continental ice sheets) in the post-LGM period will drive a sea-level rise that acts in concert with the GMSL change to submerge large sections of land that were exposed during the glacial build-up phase.

Accounting for such regional variability in RSL due to GIA is important when investigating potential coastal migration pathways and human settlement patterns (Bailey et al., 2020a; Bailey and Flemming, 2008; Bailey et al., 2007; Borreggine et al., 2022; Clark et al., 2014; Lambeck, 1996a, b; Lambeck et al., 2011), with this improved understanding of RSL being particularly important for predictive modeling of the location of now-submerged archaeological sites (Bailey et al., 2020b; McLaren et al., 2019; Veth et al., 2020). In order to inform questions about first migrations and subsequent human settlement patterns along the west coast of North America, Clark et al. (2014) computed RSL change across the California-Oregon-Washington and Bering Sea continental shelves since the LGM using an ice age sea-level theory that accurately incorporates time-varying shoreline geometry. Their main conclusions were based on an analysis of GIA using a one-dimensional (1-D) viscoelastic Earth model. However, the west coast of North America is characterized by an active plate boundary with associated variations in both lithospheric thickness (Conrad and Lithgow-Bertelloni, 2006) and mantle structure (Schmandt and Humphreys, 2010). Clark et al. (2014) provided a preliminary assessment of the impact that this complexity might have on the predictions of sea-level change and shoreline migration by running a sea-level simulation based on a three-dimensional (3-D) model of the GIA process that is capable of incorporating such features (Latychev et al., 2005). This assessment found that the 3-D predictions are shifted earlier by ~1 kyr relative to the 1-D simulation, leading Clark et al. (2014) to conclude that the sea-level simulations should incorporate the full complexity of Earth structure beneath western North America.

Clark et al. (2019) further evaluated this issue for the Oregon and Washington (OR-WA) coasts using a 3-D mantle viscosity field with a geometry constrained by seismic tomography that reflects the tectonic setting of the Cascadia subduction zone where the Juan de Fuca, Gorda, and Explorer plates subduct below North America (Fig. 1). Comparison to predictions based on a 1-D model showed significant improvement in the fit of the 3-D model to RSL observations, with the 3-D predictions shifted earlier by ~1 kyr relative to the 1-D simulation as in Clark et al. (2014).

Here we compare the Clark et al. (2014) (herein C14) and Clark et al. (2019) (herein C19) RSL predictions for the last 12 kyr and show that the C19 predictions, which are validated by RSL data, result in significant changes in coastal paleogeography compared to the C14 reconstructions. These results thus suggest that the new C19 RSL predictions that incorporate the complex 3-D solid Earth structure of the Cascadia subduction zone currently provide the most accurate paleogeographic reconstructions for the OR-WA coasts needed for predictive modeling of submerged archaeological sites in this region (McLaren et al., 2019).

## 2. Methods

We use the compilation of relative sea-level data from Engelhart et al. (2015) that provide coverage of the Oregon and Washington coasts (Fig. 1). We restrict our analysis to sites that are south of the Cordilleran Ice Sheet so as to reduce errors associated with uncertainties in the ice-sheet loading history, and north of the Mendocino triple junction so as to avoid the associated rheological complexity (Fig. 1). We also restrict our analysis to the last 12 kyr, which is the period when sufficient RSL data exist to constrain our modeling. Data corresponding to our site 1 are from site 6 of Engelhart et al. (2015), data for our site 2 are from their site 8, data for our site 3 correspond to their site 9, and data for our site 4 correspond to their site 10. These data include index and limiting points. An index point indicates formation at the RSL of the time. A limiting point indicates formation in a freshwater or marine environment such that reconstructed RSL must fall below freshwater limiting dates and above marine limiting dates (Engelhart et al., 2015).

Clark et al. (2014, 2019) described in detail the calculation of sea-level changes associated with the GIA process. The sea-level calculations were performed using an algorithm (Kendall et al., 2005; Mitrovica and Milne, 2003) that requires, as input, models for both the global geometry of ice sheets over the last glacial cycle and the Earth's viscoelastic structure. The algorithm yields a gravitationally self-consistent ocean redistribution and it accounts for the viscoelastic deformation of the solid Earth in response to the (ice plus water) loading, as well as associated perturbations to the Earth's gravitational field and rotational state (Mitrovica et al., 2005). The sea-level theory accurately treats the migration of shorelines due to local sea-level variations and changes in the perimeter of grounded, marine-based ice sheets (Milne et al., 2002), and an iterative procedure adopted within the algorithm guarantees that the predicted present-day topography matches the observed topography (Kendall et al., 2005).

The C14 predictions are based on a spherically symmetric, self-gravitating, linear (Maxwell) viscoelastic Earth model, with the elastic and density structure prescribed from the seismic model PREM (Dziewonski and Anderson, 1981). Clark et al. (2014) coupled a model of ice history developed at the Australian National University (ANU ice model) (Fleming and Lambeck, 2004) to the 1-D Earth model which has a lithospheric thickness of 96 km, an upper-mantle viscosity of $0.5 \times 10^{21}$ Pa s, and a lower-mantle viscosity of $8 \times 10^{21}$ Pa s, referred to as the ANU-LM_1D model (Muhs et al., 2012). In contrast, the C19 predictions are based on the ICE-6G ice history (Argus et al., 2014; Peltier et al.,

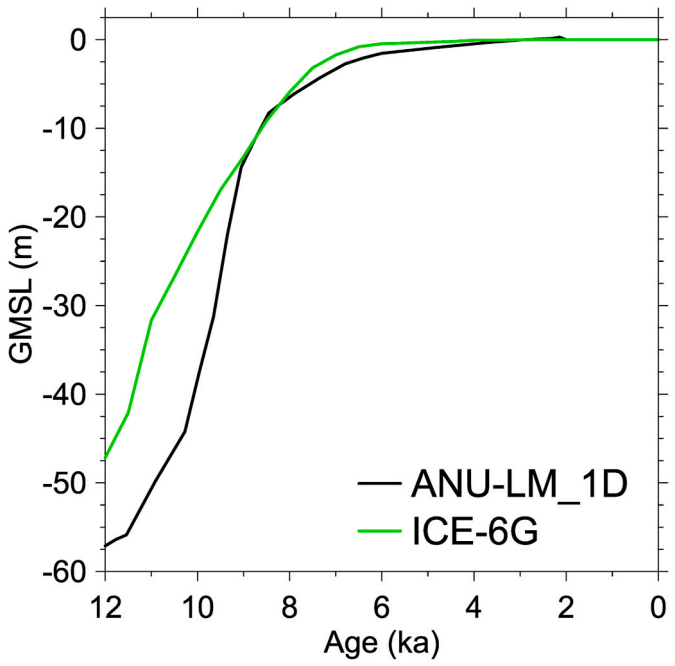


**Fig. 2.** Comparison of eustatic sea level of the ANU ice history (Fleming and Lambeck, 2004) and the ICE-6G ice history (Argus et al., 2014; Peltier et al., 2015) for the last 12 kyr.

2015). In the 1-D calculations, they coupled the ICE-6G model to the VM5a radial viscosity profile (Argus et al., 2014) which has an elastic lithosphere of thickness 90 km, an upper-mantle viscosity of $5 \times 10^{20}$ Pa s, and a lower-mantle viscosity of $1.6 \times 10^{21}$ Pa s to a depth of 1200 km and $3.2 \times 10^{21}$ Pa s below this. They then coupled the ICE-6G model to a Maxwell viscoelastic Earth model with 3-D variations in elastic lithospheric thickness and mantle viscosity (herein ICE-6G_HU_3D model). The former is based on the model of Conrad and Lithgow-Bertelloni (2006). The latter is the viscosity field preferred in Clark et al. (2019) based on its simultaneous fit to RSL records in the Pacific Northwest and post-glacial decay times over Hudson Bay (i.e., the epsilon = 0.01 case, with dimension of $1/^{o}C$). The sea-level predictions described here from the ICE-6G_HU_3D model have minor differences with the C19 results (~1 m at 10 ka) because of improvements in the GIA software.

Our GIA calculations are based on the finite-volume model described by Latychev et al. (2005) and the iterative scheme outlined by Kendall et al. (2005) for the case of Earth models with 3-D viscoelastic structure. The numerical grid has a resolution which varies from ~12 km at the surface to 50 km at the base of the mantle. In results presented below, the computed changes in sea level are superimposed onto a 3-arcsecond regional grid of modern bathymetry and topography (U.S. Coastal Relief Model http://www.ngdc.noaa.gov/mgg/coastal/crm.html) for Oregon and Washington to track changes in shoreline position as a function of time.

We note that Clark et al. (2014) compared their RSL results to the ANU eustatic sea-level history in order to illustrate the errors of using the latter to reconstruct coastal paleogeography. In contrast, Clark et al. (2019) used the ICE-6G ice history in their sea-level predictions, with the corresponding eustatic history differing from the ANU eustatic history (Fig. 2). In the following comparisons of the two studies, we thus compare the C14 RSL predictions to the ANU eustatic history (as in Clark et al. (2014)) and the C19 RSL predictions to the ICE-6G eustatic history (Fig. 3).

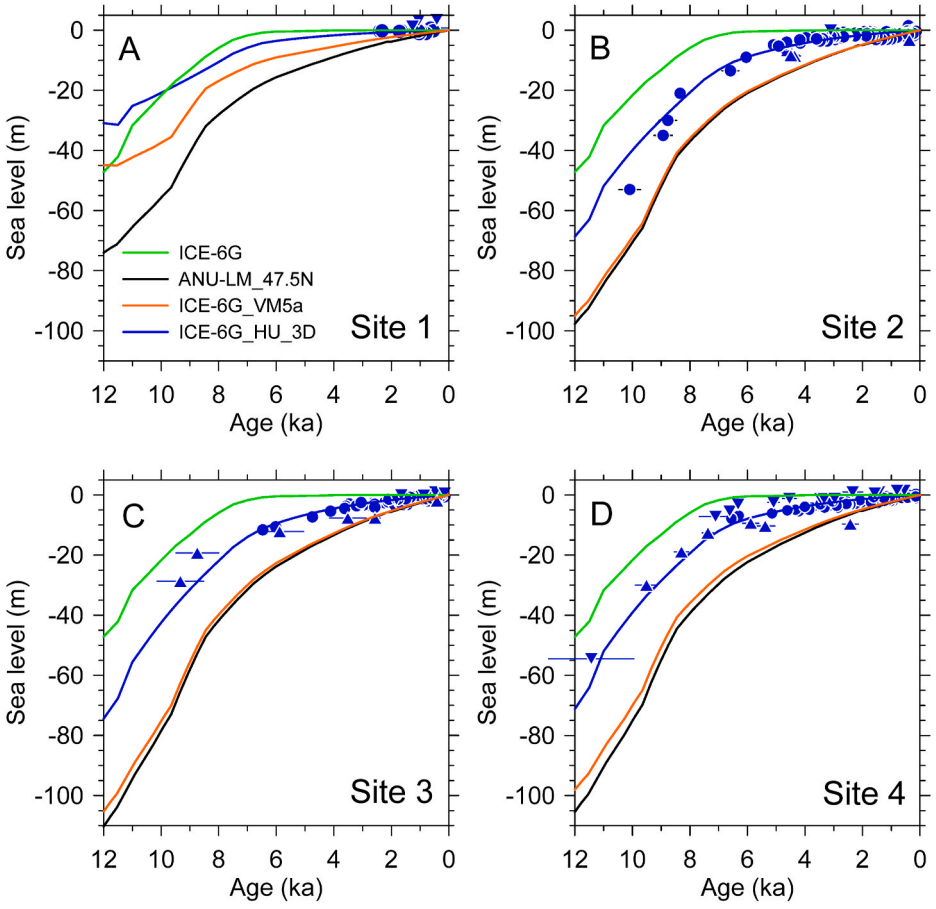


**Fig. 3.** Comparison of relative sea-level (RSL) observations (Engelhart et al., 2015) (symbols) to eustatic sea level from ICE-6G ice history (Argus et al., 2014; Peltier et al., 2015) and relative sea level based on various glacial isostatic adjustment predictions. Panels A–D refer to results and observations for sites 1–4 (Fig. 1), respectively. Results are shown for the one-dimensional Earth models LM_1D (Muhs et al., 2012) and VM5a (Argus et al. (2014), and the three-dimensional HU_3D Earth model (Clark et al., 2019), with the former based on the ANU ice history and the latter two based on the ICE-G ice history. Symbols for RSL data: circles—index points; normal triangles—maximum limiting (freshwater) points; inverted triangles—minimum limiting (marine) points.

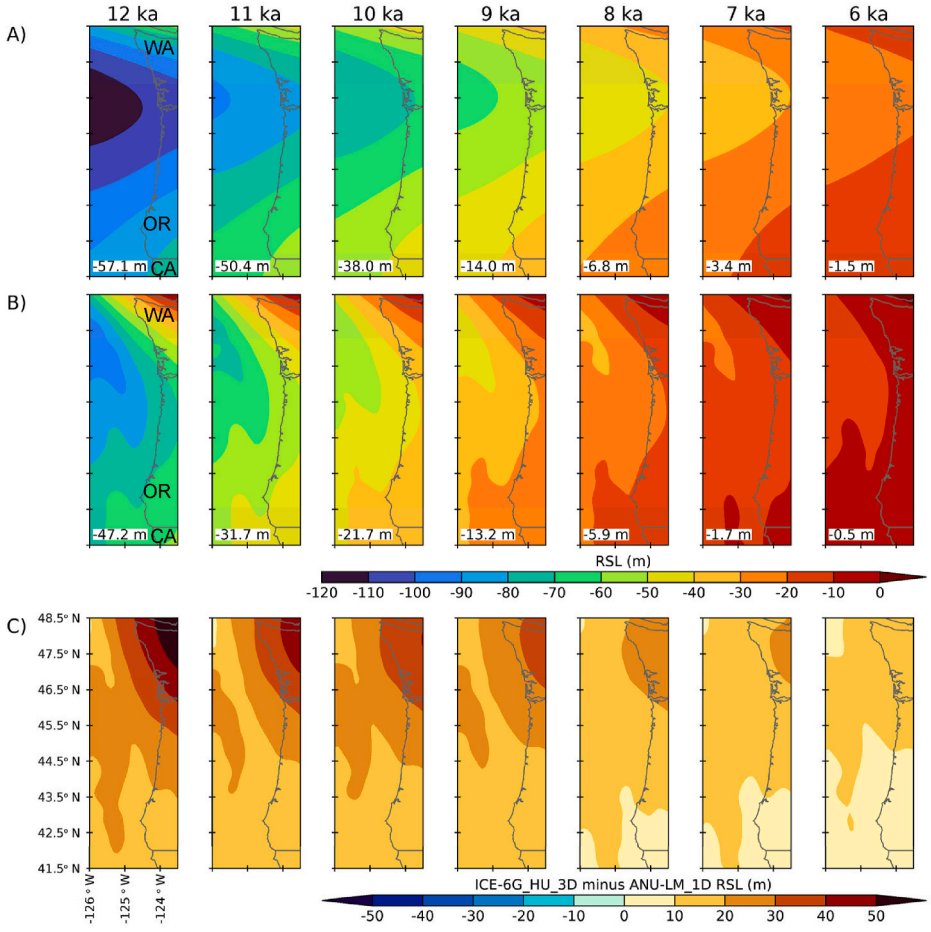


**Fig. 4.** (**A**) Regional maps of relative sea level (RSL) from 12 ka to 6 ka predicted using the gravitationally self-consistent sea-level theory and the ANU-LM_1D model of GIA (Clark et al., 2014). Corresponding eustatic sea-level value from the ANU ice history shown at lower left of each panel. (**B**) Regional maps of relative sea level (RSL) from 12 ka to 6 ka predicted using the gravitationally self-consistent sea-level theory and the ICE-6G_HU_3D model of GIA (Clark et al., 2019). Corresponding eustatic sea-level value from the ICE-6G ice history shown at lower left of each panel. (**C**) Difference maps between the two RSL predictions (ICE-6G_HU_3D RSL minus ANU-LM_1D RSL).

## 3. Results

Fig. 3 compares RSL data constraints from four areas along the OR-WA coast used in the C19 analysis (Fig. 1) (Engelhart et al., 2015) to the ICE-6G eustatic sea-level history, the RSL predictions using the ANU-LM_1D GIA model from Clark et al. (2014), and RSL predictions based on the ICE-6G ice history and either the 1-D VM5a Earth model or the HU_3D Earth model from Clark et al. (2019). The four areas lie on the peripheral bulge of the Cordilleran and Laurentide Ice Sheets and are subject to a sea-level rise associated with Holocene subsidence of the forebulge. As Clark et al. (2019) showed, however, accounting for the tectonic effects of the Cascadia subduction zone with the HU_3D Earth model results in a significantly improved fit to the RSL data for the last 8–10 kyr as compared to the VM5a 1-D Earth model; here, we extend these predictions to 12 ka. Fig. 3 also shows that, other than immediately adjacent to the Cordilleran Ice Sheet, the RSL predictions are largely insensitive to the two coupled ice-solid Earth histories based 1-D Earth models, demonstrating that the main differences in the predictions within the peripheral bulge are due to the effects of 3-D Earth structure on GIA. In general, the 1-D models predict a higher level of isostatic disequilibrium at 12 ka than the HU_3D model, with RSL predicted to be as much as 35 m lower, and a corresponding greater net sea-level rise since that time.

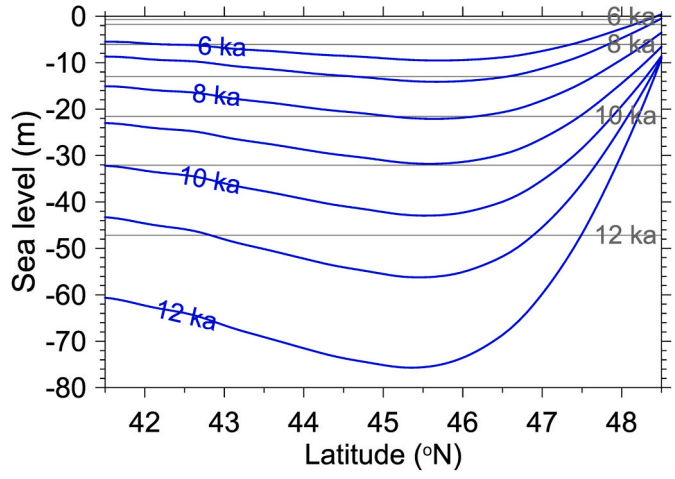


**Fig. 5.** Predictions of RSL using the ICE-6G_HU_3D model from 41.5°N to 48.5°N along 124°W from 12 ka to 6 ka (blue lines) compared to corresponding eustatic sea level value of the ICE-6G ice history (gray lines). (For interpretation of the references to colour in this figure legend, the reader is referred to the Web version of this article.)

Fig. 4 compares regional maps of the predicted RSL from 12 ka to 6 ka using the gravitationally self-consistent sea-level theory with the ANU-LM_1D model (Fig. 4A) and the ICE-6G-HU_3D model (Fig. 4B). Both predictions show similar patterns of spatially non-uniform RSL, with higher levels along the northern and southern parts of the domain and an area of lowest RSL centered on the OR-WA boundary. Whereas the spatial pattern of the ANU-LM_1D model prediction shows smoothly varying gradients of RSL, however, the spatial pattern associated with the ICE-6G_HU_3D prediction shows more variable structure that reflects the complexity of the underlying mantle structure. As seen in Fig. 3, RSL predictions from the ICE-6G_HU_3D model are everywhere higher than from the ANU-LM_1D model, again reflecting a higher level of isostatic disequilibrium in the 1-D Earth model than the 3-D Earth

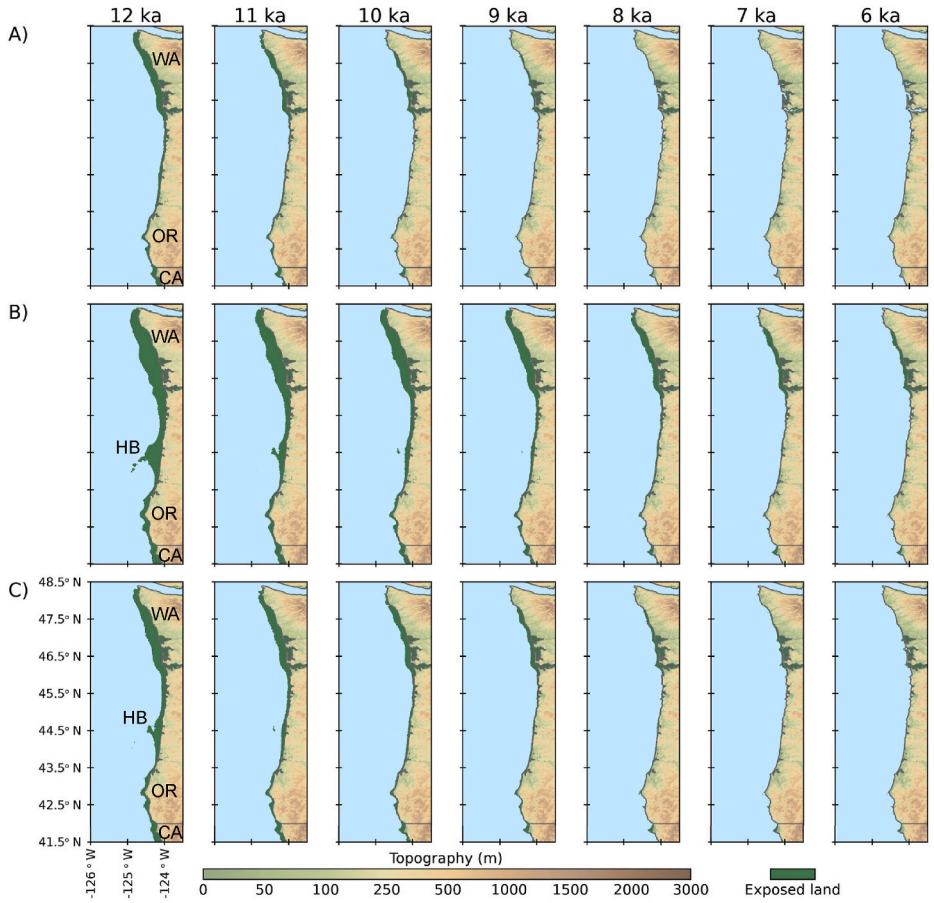


**Fig. 6.** Paleogeography of the OR-WA coast from 12 ka to 6 ka based on (**A**) eustatic sea level from ICE-6G ice history, and RSL predictions using the (**B**) ANU-LM_1D model from Clark et al. (2014), and (**C**) the ICE-6G_HU_3D model from Clark et al. (2019). HB is the Heceta Bank.

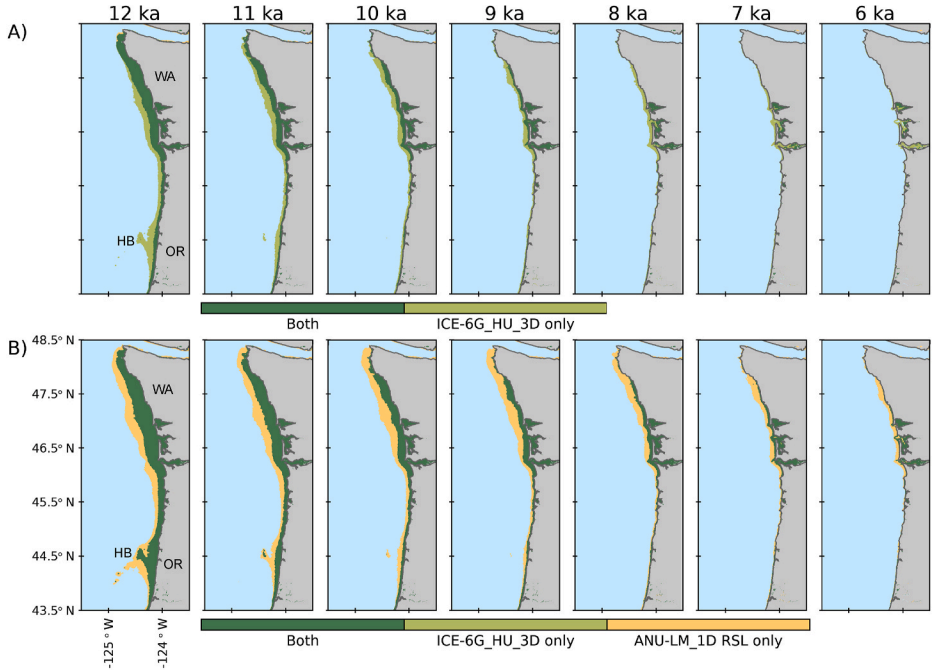


**Fig. 7.** (**A**) The difference in area of exposed shelf for the central OR and WA coast computed using the ICE-6G eustatic sea-level history and the ICE-6G_HU_3D model. Area labeled "Both" is where the two models overlap. (**B**). The difference in area of exposed shelf for the central OR and WA coast computed using the ANU-LM_1D model from Clark et al. (2014) and the ICE-6G_HU_3D model from Clark et al. (2019). Area labeled "Both" is where the two models overlap. HB is the Heceta Bank.

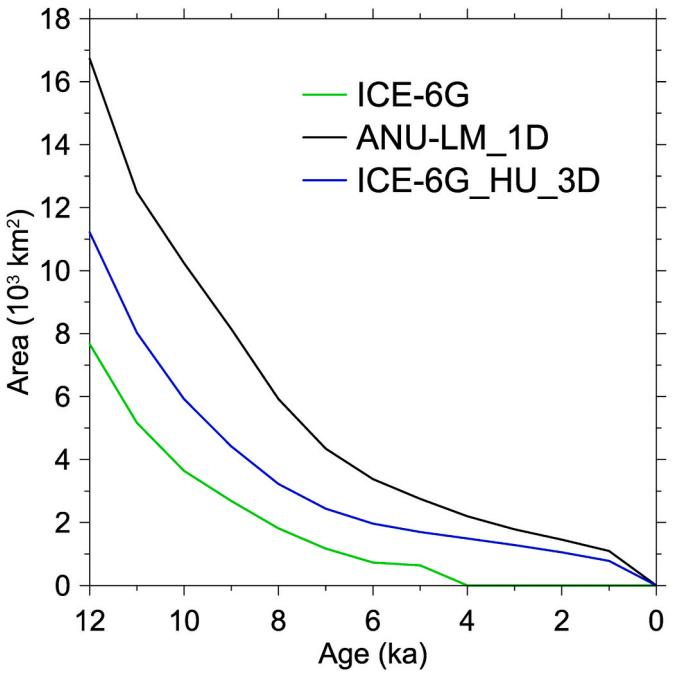


**Fig. 8.** The area of exposed shelf off the OR and WA coasts shown in Fig. 6 since 12 ka computed using the ICE-6G eustatic sea-level history, the ANU-LM_1D model, and the ICE-6G_HU_3D model.

model, with differences diminishing from 12 ka to 6 ka as isostatic equilibrium is approached in both models (Fig. 4C). This difference arises because the 3-D Earth model is characterized by a shallow zone of low viscosity (Clark et al., 2019). This structure leads to a short adjustment time for the system to ice-ocean loading such that the 3-D model simulation has adjusted closer to equilibrium by 12 ka than the 1-D simulation. The greatest differences occur in the northeastern quadrant of the domain, where RSLs at 12 ka are significantly higher by 40–50 m with the ICE-6G_HU_3D model than the ANU-LM_1D model (Figs. 3A and 4C), giving rise to a steeper gradient in RSL (Fig. 4B). These differences largely reflect differences between the ANU and ICE-6G ice histories.

The large differences in the spatial variations in RSL on the OR-WA continental shelves predicted by the ANU-LM_1D and ICE-6G_HU_3D models and their differences from eustatic (Figs. 3 and 4) demonstrate that accurate reconstructions of coastal paleogeography are highly dependent on accurately treating Earth structure in modeling the GIA process. We further illustrate this point by comparing from 12 ka to 6 ka the evolution of eustatic sea level (ICE-6G) to the latitudinal variation in RSL predicted by the ICE-6G_HU_3D model along 124°W (Fig. 5), which approximately corresponds to the modern OR-WA coastline. As evident in Figs. 3 and 4, RSL is lower than eustatic sea level along most of the coast until ~47.5°N where, because of crustal rebound (and associated sea-level fall) due to the melting of the Cordilleran Ice Sheet, RSL becomes higher than eustatic, with a total difference (RSL-eustatic) at 12 ka ranging from −30 m at 45.5°N to +38 m at 48.5°N.

Figs. 6 and 7 show how the differences between eustatic sea level and RSL associated with the ANU-LM_1D and ICE-6G_HU_3D models are expressed as coastal paleogeography from 12 ka to 6 ka. Because eustatic sea level is nearly everywhere above our RSL predictions, whereas RSL predicted by the ANU-LM_1D model is everywhere below that predicted by the ICE-6G_HU_3D model, the position of the coastline reconstructed with the ICE-6G_HU_3D model is intermediate between the reconstructions based on the ANU-LM_1D model and the assumption of eustatic sea level change. At 12 ka, the area of continental shelf exposed for the three reconstructions is 7,670 km$^2$ for eustatic, 16,730 km$^2$ for the ANU-LM_1D model, and 11,215 km$^2$ for the ICE-6G_HU_3D model, with similar differences between the reconstructions remaining until 6 ka and diminishing thereafter (Figs. 7 and 8). The largest differences between the ANU-LM_1D and ICE-6G_HU_3D reconstructions occur off the central OR coast associated with Heceta Bank, which is largely due to the hypsometry of this submerged feature, and along the Washington coast, which is primarily due to the steeper RSL gradient in the ICE-6G_HU_3D prediction than in the ANU-LM_1D prediction.

## 4. Conclusions

Late-Pleistocene sea-level changes impacted the paleogeography of

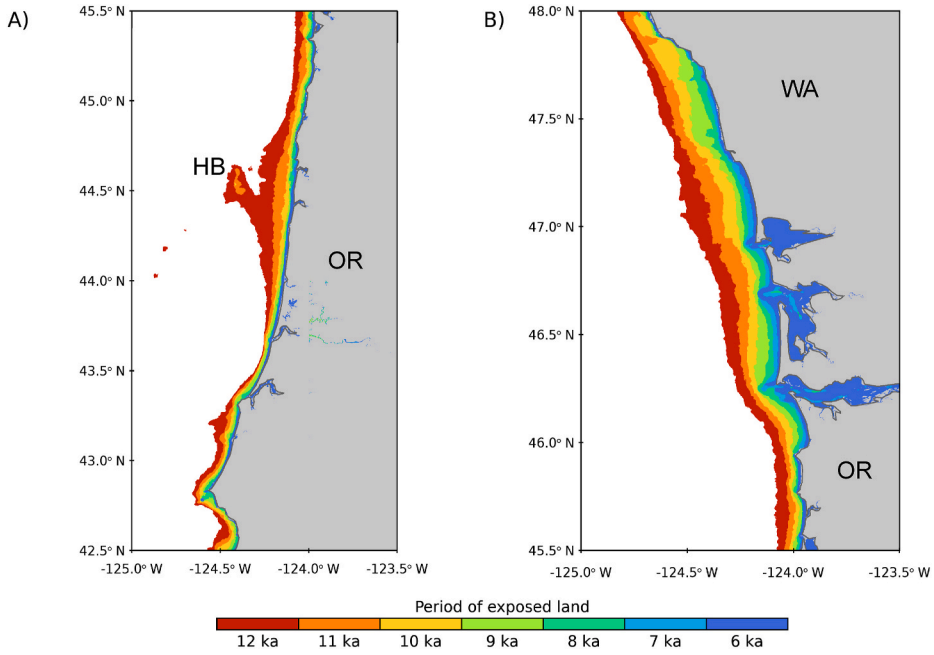


**Fig. 9.** The location of paleoshorelines on the continental shelf off the OR and WA coast from 12 ka to 6 ka at 1-kyr increments calculated using the ICE-6G_HU_3D model. (**A**) OR and WA coast between 42.5°N and 45.5°N. (**B**) OR and WA coast between 45.5°N and 48°N. HB is the Heceta Bank.

the west coast of North America and thus influenced the locations of coastal migration routes and sites of human settlement. The majority of these sites, however, are now submerged because of sea-level change, creating a significant challenge to recovering an archaeological record that is needed to test hypotheses about migrations and the influence of coastal populations on inland cultures (Davis and Madsen, 2020; McLaren et al., 2019).

A crucial step towards identifying the location of the submerged archaeological record involves having accurate predictions of changes in RSL that account for GIA (Borreggine et al., 2022; Lambeck, 1996a) and, where present, active tectonics. Using a 1-D solid Earth model, Clark et al. (2014) showed that the spatial variations in RSL from GIA cause significant departures from the previously inferred assumption of eustatic sea level, while Clark et al. (2019) showed that by accounting for the complex, 3-D structure of the Cascadia subduction zone in GIA modeling results in a significantly improved fit to the RSL data for the last 8–10 kyr as compared to the 1-D Earth model.

Here we have used the C19 RSL predictions to demonstrate the extent to which this improved modeling impacts paleogeographic reconstructions in the region. Shallow low-viscosity structure in the ICE-6G_HU_3D model leads to faster adjustment and smaller residual isostatic disequilibrium – i.e., more muted RSL change – over the past 12 kyr relative to predictions based on the ANU-LM_1D model. Thus, the reconstructed position of the coastline based on the ICE-6G_HU_3D model simulation is significantly above that based on the ANU-LM_1D model prediction, resulting in a 33% reduction in the exposed area of the 12-ka OR-WA continental shelf (Fig. 8). These reconstructions thus provide crucial information needed for predictive modeling and recovery of submerged archaeological sites in this region. For example, Fig. 9 shows the location of paleoshorelines on the continental shelf off the OR and WA coast from 12 ka to 6 ka at 1-kyr increments calculated using the ICE-6G_HU_3D model. This information forms the basis for the first two steps laid out in the strategy by McLaren et al. (2019) to identify submerged sites. Identifying the location of paleoshorelines then guides the third step in their strategy which involves developing predictive models for archaeological site discovery that are constrained by shore morphology and near-shore features such as river systems and lakes that may have influenced site location.

## Author contributions

JC conceived of the study. JRA generated the maps. MB, JXM, and KC conducted the GIA modeling. JC wrote the original draft and all authors contributed to the review and editing of the paper.

## Data availability

Datasets related to this article are available through the USGS Science Base https://doi.org/10.5066/P9171XA9.

## Declaration of competing interest

The authors declare that they have no known competing financial interests or personal relationships that could have appeared to influence the work reported in this paper.

## Acknowledgments

We thank the two journal reviewers and Summer Pretorius for their helpful comments.

## References

Anderson, D.G., Bissett, T.G., Yerka, S.J., 2013. The late-Pleistocene human settlement of interior North America: the role of physiography and sea-level change. In: Graf, K.E., Ketron, C., Waters, M.R. (Eds.), PaleoAmerican Odyssey. Center for the Study of the First Americans, College Station, TX, pp. 183–206.

Anderson, D.G., Yerka, S.J., Gillam, J.C., 2010. Employing high-resolution bathymetric data to infer possible migration routes of Pleistocene populations. Curr. Res. Pleistocene 27, 60–64.

Argus, D.F., Peltier, W.R., Drummond, R., Moore, A.W., 2014. The Antarctica component of postglacial rebound model ICE-6G_C (VM5a) based on GPS positioning, exposure age dating of ice thicknesses, and relative sea level histories. Geophys. J. Int. 198, 537–563.

Bailey, G., Galanidou, N., Peeters, H., Jöns, H., Mennenga, M., 2020a. The archaeology of Europe's drowned landscapes: introduction and overview. In: Bailey, G., Galanidou, N., Peeters, H., Jöns, H., Mennenga, M. (Eds.), The Archaeology of Europe's Drowned Landscapes. Springer Cham, Denmark, pp. 1–23.

Bailey, G.N., Flemming, N.C., 2008. Archaeology of the continental shelf: marine resources, submerged landscapes and underwater archaeology. Quat. Sci. Rev. 27, 2153–2165.

Bailey, G.N., Flemming, N.C., King, G.C.P., Lambeck, K., Momber, G., Moran, L.J., Al-Sharekh, A., Vita-Finzi, C., 2007. Coastlines, submerged landscapes, and human evolution: the Red Sea basin and the Farasan Islands. J. I. Coast Archaeol. 2, 127–160.

Bailey, G.N., Galanidou, N., Peeters, H., Jöns, H., Mennenga, M., 2020b. The Archaeology of Europe's Drowned Landscapes. Springer, Cham, Denmark, p. 561.

Bailey, G.N., Milner, N., 2002. Coastal hunter-gatherers and social evolution: marginal or central, 2002 Before Farming 1–22.

Bard, E., Hamelin, B., Arnold, M., Montaggioni, L., Cabioch, G., Faure, G., Rougerie, F., 1996. Deglacial sea-level record from Tahiti corals and the timing of global meltwater discharge. Nature 382, 241–244.

Benjamin, J., Bailey, G., 2017. Coastal adaptations and submerged landscapes: where world prehistory meets underwater archaeology. In: Monica Mărgărit, M., Boroneanț, A. (Eds.), From Hunter-Gatherers to Farmers: Human Adaptations at the End of the Pleistocene and the First Part of the Holocene. Editura Cetatea de Scaun, Romania.

Borreggine, M., Powell, E., Pico, T., Mitrovica, J.X., Meadow, R., Tryon, C., 2022. Not a bathtub: a consideration of sea-level physics for archaeological models of human migration. J. Archaeol. Sci. 137.

Clark, J., Mitrovica, J.X., Alder, J., 2014. Coastal paleogeography of the California-Oregon-Washington and Bering Sea continental shelves during the latest Pleistocene and Holocene: implications for the archaeological record. J. Archaeol. Sci. 52, 12–23.

Clark, J., Mitrovica, J.X., Latychev, K., 2019. Glacial isostatic adjustment in central Cascadia: insights from three-dimensional Earth modeling. Geology 47, 295–298.

Clark, J.A., Farrel, W., Peltier, W.R., 1978. Global changes in postglacial sea level: a numerical calculation. Quat. Res. 9, 265–287.

Conrad, C.P., Lithgow-Bertelloni, C., 2006. Influence of continental roots and asthenosphere on plate-mantle coupling. Geophys. Res. Lett. 33.

Davis, L.G., Madsen, D.B., 2020. The coastal migration theory: formulation and testable hypotheses. Quat. Sci. Rev. 249.

Davis, L.G., Punke, M.L., Hall, R.L., Fillmore, M., Willis, S.C., 2004. A Late Pleistocene occupation on the southern coast of Oregon. J. Field Archaeol. 29, 7–16.

Dziewonski, A.M., Anderson, D.L., 1981. Preliminary reference Earth model. Phys. Earth Planet. In. 25, 297–356.

Engelhart, S.E., Vacchi, M., Horton, B.P., Nelson, A.R., Kopp, R.E., 2015. A sea-level database for the Pacific coast of central North America. Quat. Sci. Rev. 113, 78–92.

Erlandson, J., 2001. The archaeology of aquatic adaptations: paradigms for a new millennium. J. Archaeol. Res. 9, 287–350.

Fairbanks, R.G., 1989. A 17,000-year glacio-eustatic sea level record: influence of glacial melting rates on the Younger Dryas event and deep-ocean circulation. Nature 342, 637–642.

Fleming, K., Johnston, P., Zwartz, D., Yokoyama, Y., Lambeck, K., Chappell, J., 1998. Refining the eustatic sea-level curve since the Last Glacial Maximum using far- and intermediate-field sites. Earth Planet Sci. Lett. 163, 327–342.

Fleming, K., Lambeck, K., 2004. Constraints on the Greenland ice sheet since the last glacial maximum from sea-level observations and glacial-rebound models. Quat. Sci. Rev. 23, 1053–1077.

Goebel, T., Waters, M.R., O'Rourke, D.H., 2008. The Late Pleistocene dispersal of modern humans in the Americas. Science 319, 1497–1502.

Hale, J.C., Benjamin, J., Woo, K., Astrup, P.M., McCarthy, J., Hale, N., Stankiewicz, F., Wiseman, C., Skriver, C., Garrison, E., Ulm, S., Bailey, G., 2021. Submerged landscapes, marine transgression and underwater shell middens: comparative analysis of site formation and taphonomy in Europe and North America. Quat. Sci. Rev. 258.

Joy, S., 2019. The trouble with the curve: reevaluating the Gulf of Mexico sea-level curve. Quat. Int. 525, 103–113.

Joy, S., 2020. Coastally-adapted: a developing model for coastal Paleoindian sites on the North American eastern continental shelf. J. I. Coast Archaeol. 16, 150–169.

Kendall, R.A., Mitrovica, J.X., Milne, G.A., 2005. On post-glacial sea level - II. Numerical formulation and comparative results on spherically symmetric models. Geophys. J. Int. 161, 679–706.

T.W. Kennett, D.J., Kennett, J.P., West, G.J., Erlandson, J.M., Johnson, J.R., Hendy, I.L., Westg, A., Culleton, B.J., Jones, T.L., Stafford, J., 2008. Wildfire and abrupt ecosystem disruption on California's Northern Channel Islands at the Ållerød–Younger Dryas boundary (13.0–12.9 ka) Quat. Sci. Rev. 27, 2530–2545.

Lambeck, K., 1996a. Sea-level change and shoreline evolution in Aegean Greece since Upper Paleolithic time, 0 Am. Antiq. 588–611.

Lambeck, K., 1996b. Shoreline reconstructions for the Persian Gulf since the last glacial maximum. Earth Planet Sci. Lett. 142, 43–57.

Lambeck, K., Esat, T.M., Potter, E.K., 2002. Links between climate and sea levels for the past three million years. Nature 419, 199–206.

Lambeck, K., Purcell, A., Flemming, N.C., Vita-Finzi, C., Alsharekh, A.M., Bailey, G.N., 2011. Sea level and shoreline reconstructions for the Red Sea: isostatic and tectonic considerations and implications for hominin migration out of Africa. Quat. Sci. Rev. 30, 3542–3574.

Latychev, K., Mitrovica, J.X., Tromp, J., Tamisiea, M.E., Komatitsch, D., Christara, C.C., 2005. Glacial isostatic adjustment on 3-D Earth models: a finite-volume formulation. Geophys. J. Int. 161, 421–444.

Lisiecki, L.E., Raymo, M.E., 2005. A Pliocene-Pleistocene stack of 57 globally distributed benthic δ18O records. Paleoceanography 20, 2004PA001071.

McLaren, D., Fedje, D., Mackie, Q., Davis, L.G., Erlandson, J., Gauvreau, A., Vogelaar, C., 2019. Late Pleistocene archaeological discovery models on the Pacific coast of North America. Paleoamerica 6, 1–21.

Milne, G.A., Mitrovica, J.X., 2008. Searching for eustasy in deglacial sea-level histories. Quat. Sci. Rev. 27, 2292–2302.

Milne, G.A., Mitrovica, J.X., Schrag, D.P., 2002. Estimating past continental ice volume from sea-level data. Quat. Sci. Rev. 21, 361–376.

Mitrovica, J.X., Milne, G.A., 2003. On post-glacial sea level: I. General theory. Geophys. J. Int. 154, 253–267.

Mitrovica, J.X., Wahr, J., Matsuyama, I., Paulson, A., 2005. The rotational stability of an ice-age earth. Geophys. J. Int. 161, 491–506.

Muhs, D.R., Simmons, K.R., Schumann, R.R., Groves, L.T., Mitrovica, J.X., Laurel, D., 2012. Sea-level history during the Last Interglacial complex on San Nicolas Island, California: implications for glacial isostatic adjustment processes, paleozoogeography and tectonics. Quat. Sci. Rev. 37, 1–25.

Peltier, W.R., Argus, D.F., Drummond, R., 2015. Space geodesy constrains ice age terminal deglaciation: the global ICE-6G_C (VM5a) model. J. Geophys. Res. Solid Earth 120, 450–487.

Schmandt, B., Humphreys, E., 2010. Complex subduction and small-scale convection revealed by body-wave tomography of the western United States upper mantle. Earth Planet Sci. Lett. 297, 435–445.

Veth, P., McDonald, J., Ward, I., O'Leary, M., Beckett, E., Benjamin, J., Ulm, S., Hacker, J., Ross, P.J., Bailey, G., 2020. A strategy for assessing continuity in terrestrial and maritime landscapes from murujuga (dampier archipelago), north west shelf, Australia. J. I. Coast Archaeol. 15, 477–503.